Local feedback mechanisms of the shallow water region around the Maritime Continent

Citation: Xue, Pengfei et al. "Local Feedback Mechanisms of the Shallow Water Region around the Maritime Continent." Journal of Geophysical Research: Oceans 119.10 (2014): 6933–6951. © 2014 American Geophysical Union

As Published: http://dx.doi.org/10.1002/2013JC009700

Publisher: American Geophysical Union (AGU)

Persistent URL: http://hdl.handle.net/1721.1/110303

Version: Final published version: final published article, as it appeared in a journal, conference proceedings, or other formally published context

AGU PUBLICATIONS

JGR

Journal of Geophysical Research: Oceans

RESEARCH ARTICLE

10.1002/2013JC009700

Special Section:
Pacific-Asian Marginal Seas

Key Points:
- Local-scale negative feedback process is identified
- The feedback is associated with short time scales of several days
- Evaporative cooling and low-level cloud feedback are the key mechanisms

Correspondence to:
P. Xue,
pexue@mtu.edu

Citation:
Xue, P., E. A. B. Eltahir, P. Malanotte-Rizzoli, and J. Wei (2014), Local feedback mechanisms of the shallow water region around the Maritime Continent, *J. Geophys. Res. Oceans*, *119*, 6933–6951, doi:10.1002/2013JC009700.

Received 3 DEC 2013
Accepted 11 SEP 2014
Accepted article online 18 SEP 2014
Published online 18 OCT 2014

Local feedback mechanisms of the shallow water region around the Maritime Continent

Pengfei Xue[1,2], Elfatih A. B. Eltahir[2,3], Paola Malanotte-Rizzoli[2,4], and Jun Wei[2,5]

[1]Great Lakes Research Center, Department of Civil and Environmental Engineering, Michigan Technological University, Houghton, Michigan, USA, [2]Center for Environmental Sensing and Modeling, Singapore-MIT Alliance for Research and Technology, Singapore, Singapore, [3]Department of Civil and Environmental Engineering, Massachusetts Institute of Technology, Cambridge, Massachusetts, USA, [4]Department of Earth, Atmospheric and Planetary Sciences, Massachusetts Institute of Technology, Cambridge, Massachusetts, USA, [5]Department of Atmospheric and Oceanic Sciences, Peking University, Beijing, China

Abstract The focus of this study is the *local-scale* air-sea feedback mechanisms over the *shallow shelf water region* (water depth <200 m) of the Maritime Continent (MC). MC was selected as a pilot study site for its extensive shallow water coverage, geographic complexity, and importance in the global climate system. To identify the local-scale air-sea feedback processes, we ran numerical experiments with perturbed surface layer water temperature using a coupled ocean-atmosphere model and an uncoupled ocean model. By examining the responses of the coupled and uncoupled models to the water temperature perturbation, we identify that, at a local-scale, a negative feedback process through the coupled dynamics that tends to restore the SST from its perturbation could dominate the shallow water region of the MC at a short time scale of several days. The energy budget shows that 38% of initial perturbation-induced heat energy was adjusted through the air-sea feedback mechanisms within 2 weeks, of which 58% is directly transferred into the atmosphere by the adjustment of latent heat flux due to the evaporative cooling mechanism. The increased inputs of heat and moisture into the lower atmosphere then modifies its thermal structure and increases the formation of low-level clouds, which act as a shield preventing incoming solar radiation from reaching the sea surface, accounts for 38% of the total adjustment of surface heat fluxes, serving as the second mechanism for the negative feedback process. The adjustment of sensible heat flux and net longwave radiation play a secondary role. The response of the coupled system to the SST perturbation suggests a response time scale of the coupled feedback process of about 3–5 days. The two-way air-sea feedback tightly links the surface heat fluxes, clouds and SST, and can play an important role in regulating the short-term variability of the SST over the shallow shelf water regions.

1. Introduction

The tropical Maritime Continent (MC) is a highly complex system, comprising many islands, peninsulas, and extensive shallow oceanic waters, adjacent to the Pacific Ocean to the east and the Indian Ocean to the west (Figure 1). With a large oceanic coverage and steep topographic gradients, water depth in this region ranges from <200 m in the shallow shelves and marginal seas (denoted by the blue contour line in Figure 1) and abruptly changing into >2000 m in the deep water of the Pacific and Indian Oceans. From an oceanic point of view, the MC is the only interocean connection at lower latitude, being the most important pathway through which the Pacific water can spread toward the Indian Ocean, transmit the El Nino-Southern Oscillation (ENSO) signal from the Pacific to the Indian Ocean, and affect the Indian monsoon system, playing an important role in the world's climate system [*Godfrey*, 1996; *Gordon*, 2005; *Qu et al*., 2009; *Tillinger and Gordon*, 2010].

From the perspective of the atmosphere, the MC is also a vitally important region located at the rising branch of the global Walker atmospheric circulation and the western edge of the Pacific oceanic "warm pool." The MC has long been described as a "boiler box" [*Ramage*, 1968] featuring large inputs of heat and moisture into the upper troposphere through intensive convective processes, as a primary energy source for global atmospheric circulation and rainfall formation [*Ramage*, 1968; *Neale and Slingo*, 2003].

Ocean-atmosphere coupling is one of the main processes shaping oceanic and atmospheric phenomena and the resulting climate dynamics in the tropics at a wide range of spatial and temporal scales. The MC, as

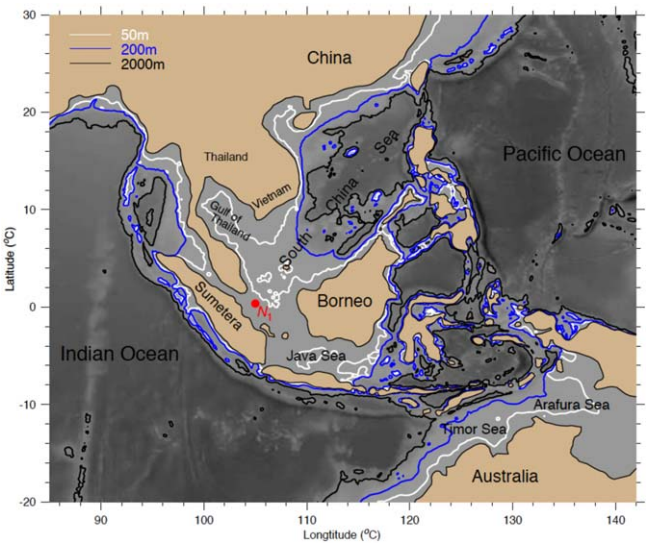

Figure 1. Bathymetry of Maritime Continent and adjacent regions. Symbols N_1 denote a sampling location selected for experiments (see text).

one of the key regions in the tropics, exhibits strongly coupled air-sea interactions. Theories on the ocean-atmosphere feedback mechanisms for the tropical region have mainly focused on the large ocean-basin scale processes related to the climate modes (e.g., Madden-Julian Oscillation (MJO) and ENSO). For example, *Bjerknes* [1969] first proposed his famous positive feedback hypothesis that the easterly winds shoal the thermocline eastward and strengthen SST gradient across the Pacific tropics, in turn stronger SST gradients lead to stronger easterly winds. *Xie and Philander* [1994] proposed the positive wind-evaporation-SST feedback by considering a scenario of a meridional dipole of SST perturbations (positive north and negative south of the equator) under the prevailing easterly trades to explain the asymmetry of the northward-displaced rain bands over the eastern Pacific and Atlantic. *Ramanathan and Collins* [1991] proposed a negative clouds feedback mechanism that cirrus clouds can regulate SST maxima in "warm pool," in which ocean warming enhanced deep convection, leading to the formation of extensive cirrus clouds shielding troposphere and reducing incoming solar radiation. *Zhang et al*. [1995] further argued that the long-term average effect of convection may even suppress the surface evaporation at very high SST ($>30^{\circ}$C) since high SST could give rise to more convective activities, which increase the low-level large-scale convergence through interactions with the large-scale circulations and therefore decrease the surface winds, leading to low evaporations in spite of the increased surface-air humidity differences. Review articles on large-scale ocean-atmosphere interactions include *Wang et al*. [2004], *Fedorov* [2008], and *Chelton and Xie* [2010]. The nature of feedback processes at different spatiotemporal scales compared with the present study is further discussed in section 5.

More recently, the rapid development of numerical models and their applications resulted in the recognition of coupled ocean-atmosphere models as some of the most important tools for studying air-sea interactions. A number of studies have been devoted to improve our understanding of the air-sea coupling process. For example, studies demonstrate how the influence of processes with regional scales can be linked or cascaded to the basin and global scale, low frequency variability of the climate system through air-sea interactions [*Slingo et al*., 2003; *Wang et al*., 2000, 2006; *Bernie et al*., 2007, 2008; *Xie et al*., 2009; *Yuan et al*., 2011; *Masson et al*., 2012]. These studies underline the importance of atmospheric feedbacks and the resultant rectification of the mean state of SST [*Bony et al*., 2004; *Danabasoglu et al*., 2006; *Lloyd et al*., 2011], and also the role of oceanic processes [*Meehl et al*., 2001; *Koch-Larrouy et al*., 2010; *Ham et al*., 2010; *Yuan et al*., 2013]. All these studies were conducted with a focus on large-scale interactions at the ocean-atmosphere interface in the tropics.

While the large-scale ocean-atmosphere interactions in the open ocean have received more attention, this study focuses on the other side of the coupled dynamics: what could the air-sea feedback be in *shelf* (*shallow water*) *regions*? What is its role in regulating the local system? Unlike open oceans, where the ocean-basin scale circulations and other large-scale processes play an important role in regulating the variability of the water properties and are therefore characterized with relatively longer correlation time scales, the continental shelf regions are often dominated with the submesoscale processes at shorter time scales, experiencing strong mixing through wind, waves, and tides, and influenced by coastal circulations and transports, of which all may impact the air-sea feedbacks. It is still unclear how and at which spatiotemporal scale the air-sea feedback in the shallow shelves could impact the energy transfer in the coupled ocean-atmosphere system and modify associated thermal structure of the atmosphere and ocean.

To address these questions, we selected the shelves and marginal seas of the MC (where water depth <200 m) as our study site. It was chosen for two important reasons: first, MC has its aforementioned geographic complexity and importance in the global climate system. Despite its important role in the regional and global climate system, current predictions of climate change over the MC still contain a high degree of uncertainty, indicating that the mechanisms driving this coupled system are still not well understood [*Christensen et al*., 2007]. Second, although numerous ocean-only or atmosphere-only modeling studies have been accomplished in this region, few modeling studies were carried out using a coupled regional ocean-atmosphere model approach [*Aldrian et al*., 2005; *Wei et al*., 2013]. These coupled modeling studies have demonstrated the importance of using model coupling approach in this region for more accurate simulations of both atmospheric and oceanic phenomena, suggesting that resolving coupled air-sea processes are crucial in the MC.

In this paper, we study the local-scale air-sea feedback processes in the shallow shelf water region of the MC using a high-resolution coupled regional ocean-atmosphere model. We first ran coupled and uncoupled models with perturbed SST fields to explore the existence of a local air-sea feedback process. By analyzing the responses of a coupled ocean-atmosphere model and an uncoupled ocean model to the SST perturbation and tracking the transfer and redistribution of the perturbation-induced heat and moisture in the ocean, atmosphere and between, we explore the associated two-way air-sea feedback mechanisms. A set of experiments was carried out to examine dynamical connections between the time scale of this local air-sea feedback process and the coupled model behavior under different SST coupling frequencies.

The remaining part of this paper is organized as follows. In section 2, the coupled ocean-atmosphere model and design of the numerical experiments are described. In section 3, process-oriented experiments with perturbed SST fields are performed using coupled and uncoupled models. The heat transfer and energy budget associated with the feedback process are quantified, and the mechanisms for the air-sea feedback are explored. In section 4, experiments with different SST coupling frequencies are carried out. Spectral analysis is conducted to examine the growth pattern of the coupling error with the variation of the SST coupling frequency. A discussion of the results is presented in section 5 and the conclusions are summarized in section 6.

2. Methods and Approaches

2.1. The Coupled FVCOM/MRCM Model

The coupled model was developed using the Finite Volume Coastal Ocean Model (FVCOM) as the oceanic component and the MIT Regional Climate Model (MRCM) as the atmospheric component. FVCOM is an unstructured-grid, finite-volume, three-dimensional primitive equation coastal ocean model [*Chen et al*., 2003, 2006], with the merit of an unstructured grid for ideal geometrical fitting and topological flexibility, which made it particularly suited for research and applications in estuarine and coastal regions featuring complex coastlines and steep topographies [*Zheng et al*., 2003; *Weisberg and Zheng*, 2006; *Isobe and Beardsley*, 2006; *Chen et al*., 2008, 2012; *Yang and Khangaonkar*, 2009; *Zhao et al*., 2010; *Xue et al*., 2009, 2011, 2012, 2014].

The MC-FVCOM was first developed for the study of Indonesian throughflow and South China Sea throughflow [*Xu and Malanotte-Rizzoli*, 2013] and has been upgraded as the oceanic component of the coupled model system over the MC [*Wei et al*., 2013]. The external and internal mode time steps of MC-FVCOM were 60 and 600 s, respectively. The model has a horizontal resolution varying from 7 to 10 km near the shelf break and along the coastlines to 50–200 km in the deep ocean near the open boundary (Figure 2), with 30 vertical layers configured with a generalized sigma coordinate. The varying thicknesses of vertical layers in this generalized sigma coordinate were specified as such to allow more near-surface layers to resolve the upper layer dynamics [*Wei et al*., 2013]. The thickness of the first layer was configured as <20 cm where the local water depth was <200 m, so that modeled surface layer temperature at our target region, i.e., the shallow water region, can be a reasonable representation of SST. Meanwhile, the thickness of the model surface layer in the deep water (water depth ranges from 200 to 6000 m) was configured between ~0.2 and 6 m (i.e., 1/1000 of local water depth), which was set to allow the model to be balanced between resolving the surface mixed layer and ensuring model stability. The open boundary forcing of sea level, temperature, and salinity were provided by the global MIT-OGCM [*Hill and Marshall*, 1995; *Marshall et al*., 1997], and

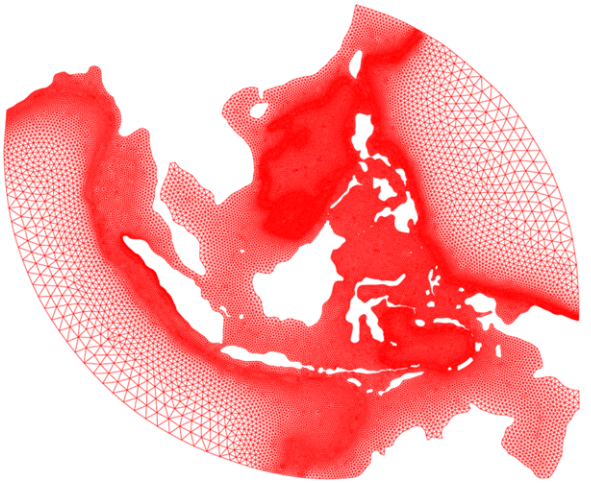

Figure 2. Unstructured grid of the Maritime Continent-FVCOM model.

atmospheric forcing of wind, surface heat fluxes (incoming solar radiation, net surface longwave radiation, latent, and sensible heat) were provided by the coupled atmospheric model: MC-MRCM.

MRCM has been developed during the last decade based on the Regional Climate Model version 3 (RegCM3) [*Giorgi and Mearns*, 1999; *Pal et al*., 2007] with a focus on improving the skill of RegCM3 in simulating climate over different regions through the incorporation of new physical schemes or modification of original schemes. One of the important features of the MRCM is the introduction of a new convective cloud and rainfall autoconversion scheme, which has been reported as a critical improvement in simulating convective-radiative feedback [*Gianotti and Eltahir*, 2013a, 2013b], being potentially important for resolving the ocean-atmosphere coupled dynamics in this region as it has a very strong convective clouds formation.

The MC-MRCM was first developed to study the convective clouds and rainfall processes over the MC [see *Gianotti et al*., 2012; *Gianotti and Eltahir*, 2013a, 2013b]. In all simulations presented, the model time step was set to 120 s with the land surface scheme was run every 360 s. In the original MC-MRCM, ocean surface fluxes, handled by Zeng's bulk aerodynamic ocean flux parameterization scheme [*Zeng et al*., 1998], were computed from the Global sea-Ice and Sea Surface Temperature (GISST) data set with monthly and $1^\circ \times 1^\circ$ resolution, while in the coupled model SST fields are provided by the coupled MC-FVCOM.

The FVCOM and MRCM are coupled using the OASIS3 software, which is designed to implement end-to-end coupling of different numerical models in a parallelized computation environment [*Valcke et al*., 2004]. FVCOM and MRCM are integrated forward simultaneously and OASIS3 interpolates and transfers the coupling fields from the source grid to the target gird at a specified coupling interval (coupling interval is alternatively termed with "coupling frequency," e.g., SST coupling frequency refers to how often the MC-FVCOM provides SST to MC-MRCM).

2.2. Data

The data sets used for analysis include long-term NCEP reanalysis monthly mean wind speed with $2.5 \times 2.5^\circ$ resolution [*Kalnay et al*., 1996], derived from the data available for years 1981–2010, NOAA Optimum Interpolation long-term monthly mean SST (OISST) [*Reynolds et al*., 2002] with 1×1 degree resolution, derived from the data available for years 1971–2000, and the Australian Multi-Sensor SST Analysis (RAMSSA) [*Beggs et al*., 2011] which has a very high spatial resolution of 9 km $\times$ 9 km covering the region (20N–70S, 60E–170W), the drawback was that it was not available until year 2008, so it was only used here to verify the general SST spatial variability during the discussion.

2.3. Design of Experiments

When the coupled model was first developed, a 20 year (1960–1980, with 60 s for spin-up and 70 s for analysis) coupled simulation of the MC has been made with comprehensive model-data comparisons to validate the model performance [*Wei et al*., 2013]. In the coupled model system, the ocean model MC-FVCOM provides the SST (represented by the surface layer temperature of MC-FVCOM) to the atmospheric model MC-MRCM as its lower boundary condition and the atmospheric model MC-MRCM provides the surface heat fluxes and wind fields to the ocean model MC-FVCOM as its surface forcings once every 6 h through the coupler OASIS3. We refer interested readers to *Wei et al*. [2013] for the development of the coupled model, detailed coupling techniques, and model validation. We inherited the coupled model simulation of *Wei et al*. [2013] so that there is no need to represent the model validation in this study. To keep this paper concise, we directly refer to it as the "control run" and the model results are treated as "reference state."

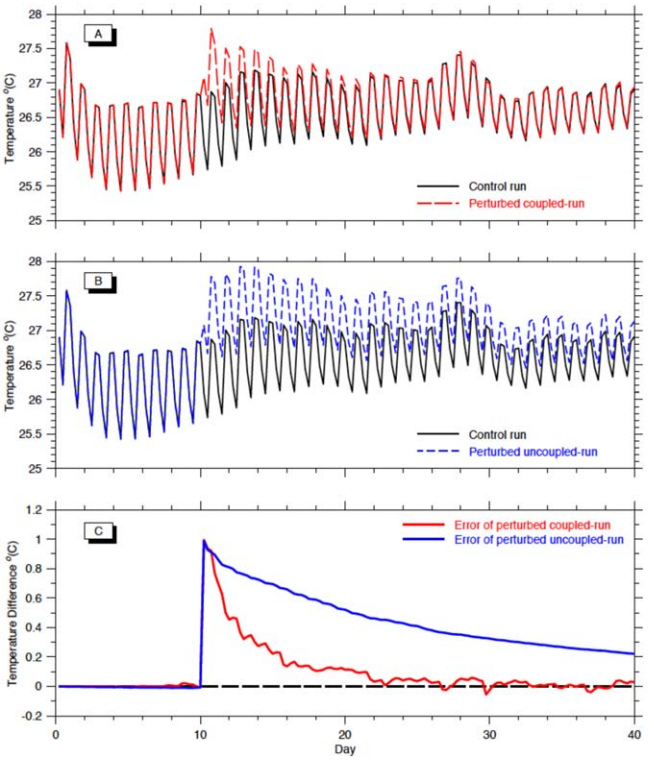

Figure 3. Time series of SST averaged over the shallow water regions (a) for case *I* (coupled case) and "control run", and (b) for case *II* (uncoupled case) and "control run" in Ex#1. (c) Changes of the SST for cases *I* and *II* relative to the "control run".

An experiment (Ex#1) with water temperature perturbations in the surface layer was designed to identify the local air-sea feedback mechanism and the response time scale of the feedback process over the shallow water region of the MC. The model was run with the same configuration as in the "control run" for 10 days and a perturbation was imposed to the temperature field at the upper 10 m in the shallow region. In order to focus on the atmospheric response to the ocean perturbation, we chose a positive rather than a negative perturbation, as a negative perturbation of water temperature causes the convective process of the near surface water, which further complicates the dynamics by adding ocean convective adjustments in addition to air-sea adjustments. In this experiment, temperature at upper 10 m was artificially increased by 1°C in the region with water depth $\leq$200 m; no perturbation was made in the region with water depth $\geq$500 m; a linear transition of SST perturbation was used in the region with water depth between 200 and 500 m. In the first case (case *I*), we continued to run the coupled model; and in the second case (case *II*), we ran the uncoupled ocean-only model with prescribed surface forcings obtained from the "control run."

Furthermore, if this air-sea feedback is of significance, resolving the response time scale of the feedback process in a coupled model will be a critical condition in properly simulating the SST variability over this region. As we speculate that the local-scale feedbacks may exhibit with a time scale that may be comparable to that of meso or submesoscale coastal processes, we designed an experiment (Ex#2) by running the coupled model with different coupling frequencies of SST to test the stated hypothesis. In the aforementioned "control run," the coupling frequencies of SST, surface heat fluxes, and wind fields are all 6 h. In this experiment (Ex#2), we reran the coupled model with the same model configuration as in the "control run" but changing the SST coupling frequency to daily (case *a*), or weekly (case *b*). In this diagnostic experiment, we intentionally kept the coupling frequencies of the winds and surface heat fluxes unchanged (6 h) so that we can solely focus on the influence of the change in SST coupling frequency on the model behavior, and keep the unchanged contribution of the diurnal solar forcing to the coupled system. A similar approach has been used by *Masson et al*. [2012] and *Terray et al*. [2011] to study the impact of intradaily SST variability on ENSO characteristics and the role of the intradaily SST variability in the Indian monsoon variability, respectively. It should be noted here that testing different SST coupling frequencies in Ex#2 was for understanding the dynamical connection between the coupling feedback process and the model behavior, rather than an attempt to technically optimize model coupling frequency.

3. Negative Feedback Process of the Coupled System

Results of experiment (Ex#1) are presented in Figure 3. In case *I*, SST tended to restore back to the "reference state" from its perturbation at a very fast rate, the coupled system was able to almost completely correct itself in ~15 days. In contrast, when the two-way air-sea feedback process was disallowed in case *II*, the uncoupled model took a much longer time to adjust. The *e*-folding time scale of the error reduction in

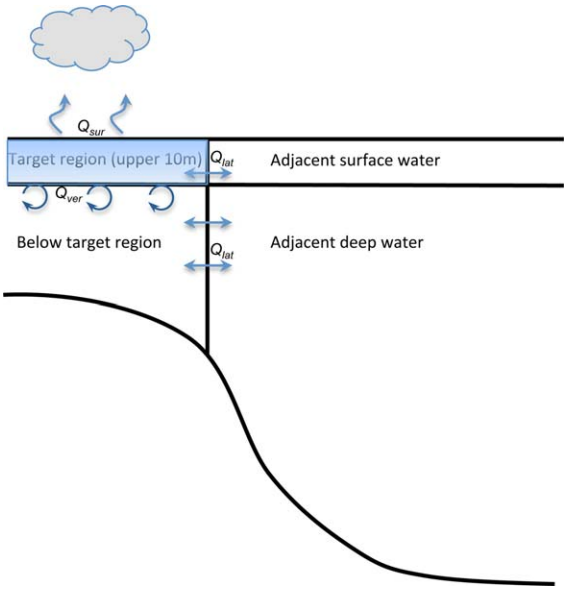

Figure 4. Schematic of the perturbation-induced heat transfer and redistribution in the ocean and atmosphere.

case *I* (~4 days) and case *II* (~20 days) clearly show the critical role of the two-way air-sea feedback process in self-regulating the coupled system, suggesting a *negative* air-sea feedback process over the shallow water region of the MC which tends to restore the SST from its perturbation and help stabilize the system, with a response time scale ~3–5 days.

3.1. Energy Budget and Feedback Mechanisms

The perturbation of water temperature in Ex#1 introduces additional heat content into the coupled system, which is initially stored in the water surface layer in the shallow shelf region. The response of the atmosphere and ocean to the perturbation in the coupled system results in a redistribution of heat. By tracking this redistribution, we identify the role of the atmosphere and ocean in shaping the physical mechanisms of air-sea feedback processes and quantify the impact of this energy transfer on the thermal structure of the atmosphere and ocean.

3.1.1. Energy Budget in the Ocean

As a result of temperature perturbation within the near-surface (upper 10 m) layer in the shallow waters ($\leq$200 m), the perturbation-introduced heat amount can be calculated as:

$$Q_0 = c \cdot \rho \cdot V \cdot \Delta T \tag{1}$$

where Q_0 is the initial perturbation-induced heat content in the "target region" (water column in the upper 10 m of shallow water region $<$200 m), c, ρ, and V are the specific heat capacity, density, and water volume of seawater, and ΔT is the perturbation in water temperature (1°C in Ex1), which generated a total perturbation-induced heat energy (Q_0) ~1.93e^{20} J.

This initial perturbation-induced heat in the target region is consequently transferred and redistributed through a combination of three different processes: Q_{sur} is the heat transported into atmosphere through surface heat fluxes, Q_{ver} and Q_{lat} are the heat transported downward to the water column below the target region through vertical mixing and into the adjacent water through lateral heat exchange by advection and eddy diffusion. A schematic of the transfer of the perturbation-induced heat is presented in Figure 4.

Using a formula similar to equation (1), the removal of the initial perturbation-induced heat content ($-d(Q_0)$) from the target region over a period of time ($dt = t_0 - t_n$) from the initial perturbation (time t_0) is calculated as:

$$-d(Q_0) = \sum_{i=1,m} c \cdot \rho_i \cdot V_i \cdot \Delta T_i^{p-c} \tag{2}$$

where $\rho_i \cdot V_i$ and ΔT_i^{p-c} are the density, water volume, and the water temperature difference between the case *I* and "control run" at the time t_n on the m model grid control volumes ($i = 1, m$) in the target region. Similarly, we track the increase of heat in the water column below the target region $d(Q_1)$, which is a reflection of the heat being transferred downward from target region through mixing Q_{ver} and exchange with adjacent deep water

$$d(Q_1) \approx \sum_{k=1,n} c \cdot \rho_k \cdot V_k \cdot \Delta T_k^{p-c} \tag{3}$$

where $\rho_k \cdot V_k$, ΔT_k^{p-c} is the density, water volume, and water temperature difference between the case *I* and "control run" at the time t_n on n model grid control volumes that are below 10 m of the shallow water

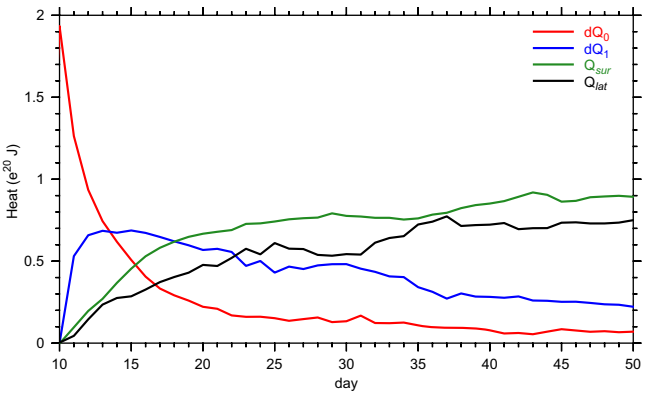

Figure 5. Time series of the transfer and redistribution of the perturbation-induced heat energy in the target region ($-dQ_0$), receipt of heat in the water column below the target region (dQ_1), the adjustment of surface heat fluxes (Q_{sur}), and lateral heat exchange with ambient water Q_{lat}.

region. Q_{lat} is estimated from the model's advective and diffusivity terms in the temperature equation across the section.

The heat budget from the sea surface Q_{sur} is determined by the net effect of the latent heat flux, sensible heat flux, outgoing longwave radiation, downward longwave radiation, and incoming/reflected shortwave radiation. All of these flux components are calculated in the coupled model using the ocean flux model [*Zeng et al.*, 1998], which will be elaborated in the next section.

Figure 5 presents the cumulative adjustment of heat over time from the target region in the coupled system (case *I*). The perturbation-introduced heat in the target region was reduced by ~73% from an initial 1.93e^{20} J into 0.51e^{20} J within the first 5 days (day 11–day 15), further reduced by 18% (day 15–day 24) and only 9% of initial perturbation-induced heat remains within the target region after 2 weeks. This quick reduction of heat in the target region shows a close agreement with the SST restoration pattern in Figure 3. The surface heat flux through the air-sea interaction removes ~0.74e^{20} J within 14 days, accounting for ~38% of the total adjustment of the perturbation-induced heat. The heat transfer downward is evident in the increase of heat in the water column below the target region. A rapid increase in the heat content $d(Q_1)$ occurs within the first 3 days, indicating a significant downward heat transfer through vertical mixing due to the large temperature gradient from the initial perturbation. The cumulative heat below the target region reached its peak value 0.68e^{20} J, implying that at least 35% of total perturbation-induced heat was transferred downward. After 5 days, as the surface water temperature is being restored from its perturbation and the vertical heat transfer decreases, lateral transport of heat to ambient water outweighs the receipt of heat from vertical transfer, 0.5e^{20} J (25%) remaining in the water column below the target region after 14 days. Total lateral heat transfer with adjacent water accounts for ~28% of the total transfer of perturbation-induced heat energy within 2 weeks.

In the uncoupled simulation (case *II*), the adjustment of surface heat flux through air-sea interaction is disallowed since the surface heat flux driving the ocean model was prescribed. The transfer and redistribution of the initial perturbation-induced heat can only be achieved through the vertical mixing and later advection and eddy diffusion, which make the adjustment of the SST restoration much slower. Over 15% of the perturbation remained even after 3 months of simulation, with the residual errors persisting in the Gulf of Thailand, Java Sea, and Arafura Sea, where the water lateral and vertical exchange to the ambient ocean was limited (Figures 3 and 6).

3.1.2. Energy Budget in the Atmosphere

In Ex#1, 38% of the perturbation-induced heat was transferred over the shelf water region into the atmosphere through the air-sea interaction within 14 days. The heat budget from the sea surface is controlled by the net effect of the latent and sensible heat fluxes, upward and downward longwave radiation and incoming/reflecting shortwave radiation, which are determined by oceanic and meteorological conditions including air and sea temperature, humidity, cloud coverage, and wind speed. This section is aimed at quantifying their roles in air-sea interactions and their impact on the thermal structure of the atmosphere.

3.1.2.1. Latent and Sensible Heat Fluxes

Due to high evaporation rates in the tropics, the surface energy balance is dominated to a large degree by the latent heat flux, which typically has a value that is at least 1 order of magnitude larger than the sensible heat flux and net surface longwave radiation. Figure 7 presents the 5 day averaged latent heat comparison after SST perturbation between the perturbed run and control run. During the boreal winter, the northern MC in the Pacific Ocean typically has stronger evaporation and the resulting latent heat usually reaches $\geq$200 W/m^2, while in the Indian Ocean it is usually $\leq$120 W/m^2 (top).

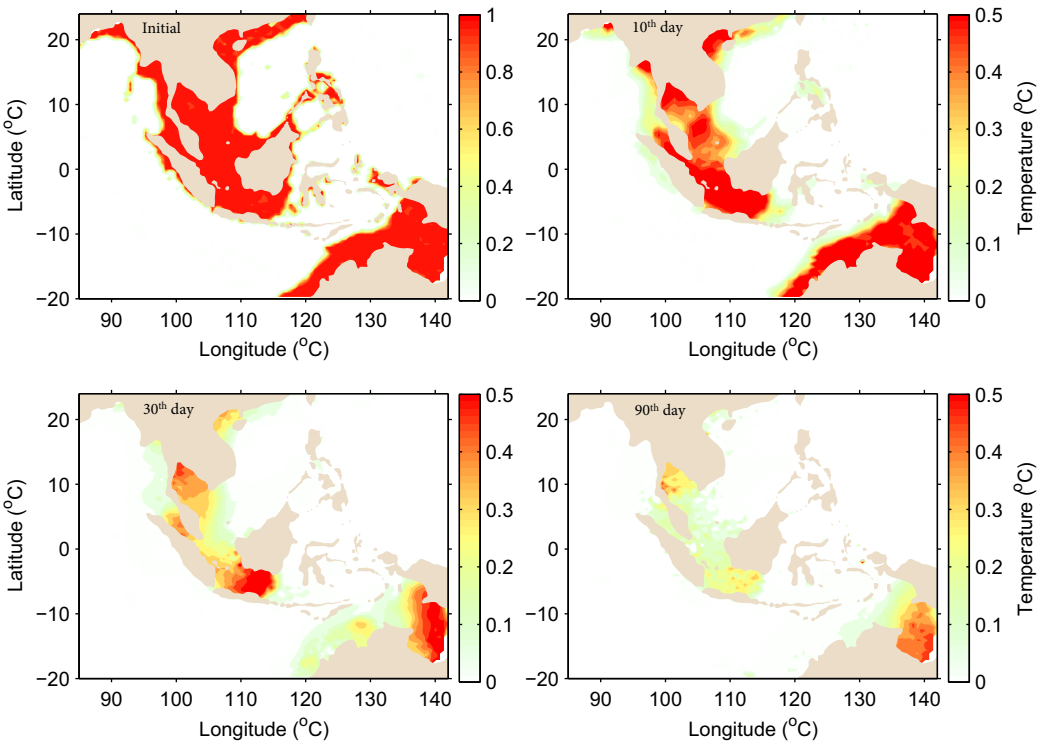

Figure 6. Distribution of surface water temperature perturbation in the case *II* (uncoupled case) of Ex#1 at the initial day, 10th day, 30th day, and 90th after the initial perturbation.

The middle and bottom plots in Figure 7 reveal the adjustment of latent heat flux in response to the SST perturbation in the coupled system. An average of ~13 W/m^2 increase in the latent heat occurred within the first 5 days after the initial SST perturbation in the shallow water region. The adjustment of latent heat starts with its peak value of 33 W/m^2 after the SST perturbation with the magnitude of latent heat adjustment decreasing over time. Significant adjustments have been made over the first 5 days, suggesting that the SST-latent heat adjustment serves as the first important mechanism in the feedback process in the MC.

This latent heat response is consistent with the evaporative cooling process [*Hartmann and Michelsen*, 1993]. Using the bulk formula of the latent heat flux (H_l)

$$H_l = \rho_a L_e C_e U_{10}(q_s - q_a) \tag{4}$$

where ρ_a is the air density (~1.5 kg/m^3), L_e is the latent heat of evaporation (~2.5·10^6 J/kg), C_e is the latent heat transfer coefficient (~1.35·10^{-3}), U_{10} and q_a are the wind speed and the specific humidity of air at the 10 m reference level above the sea surface, and q_s is the saturated specific humidity over saline seawater, formulated as:

$$q_s = 0.98 q_{sat}(T_s) \tag{5}$$

where T_s is the sea surface temperature and q_{sat} is the saturation specific humidity for pure water at T_s. The factor of 0.98 is an approximation to take into account the reduction of vapor pressure caused by a typical ocean salinity of 34 [*Kraus and Businger*, 1994], where q_{sat} follows the formula in *Buck* [1981],

$$q_{sat} = \frac{0.622 e_s}{P_a - 0.378 e_s} \tag{6}$$

$$e_s = [1.0007 + (3.46 \cdot 10^{-6} P_a)] \cdot 6.1121 \exp\left(\frac{17.502 T_s}{240.97 + T_s}\right) \tag{7}$$

where P_a is the air pressure. Considering a perturbation of SST from $T_s \rightarrow T_s'$, the instant adjustment of latent heat flux can be estimated by

$$\Delta H_l = \rho_a L_e C_e U_{10} 0.98 [q_{sat}(T_s') - q_{sat}(T_s)] \tag{8}$$

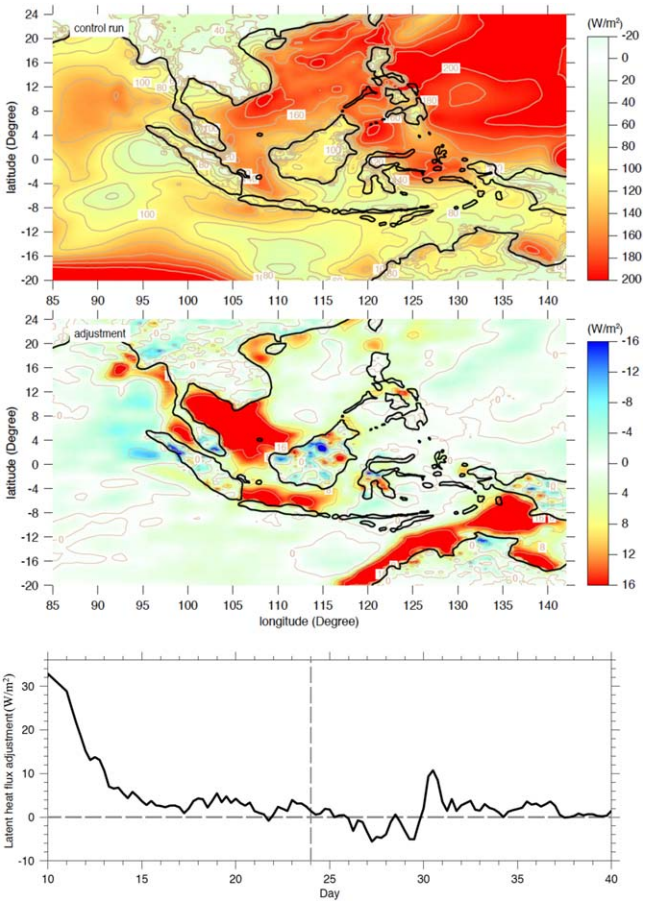

Figure 7. (top) Distribution of the latent heat flux in the control run, (middle) the increase in the latent heat flux 5 day average after initial water temperature perturbation in case *I*, and (bottom) the time series of the adjustment of the latent heat flux averaged over the shallow water region.

Calculated from 30 year NCEP reanalysis and OISST long-term monthly data, the monthly wind speed over the shallow water regions varies between 3.5 and 5 m/s, with higher wind speed during boreal winter and summer and lower during spring and fall (Figure 8, top). The monthly SST varies between 27 and 29°C. Given the climatological wind speed at 5 m/s and SST of 27°C for the perturbation experiment in January 1971, the latent heat adjustment is estimated to be ~36 W/m^2 for a perturbation of 1°C, in a good agreement with the model response. The magnitude of the adjustment of the latent heat flux caused by the increase of SST by 1°C ranges from ~20 to 40 W/m^2 under combinations of different baselines of SST and wind speed, as shown in the bottom plot of Figure 8. Such a simplification as shown in equation (8) holds for the 1-D vertical response at short time scales as discussed here [*Zhang et al*., 1995], while at the large spatial scale and long time scales (e.g., intraseasonal), the change in wind and atmosphere temperature in response to SST anomaly must be included, a scaling analysis at intraseasonal scale is presented in *Small et al*. [2011]. Using TOGA-TAO buoys in the equatorial western Pacific, *Zhang et al*. [1995] and *Wang and McPhaden* [2001] investigated the intraseasonal variability of the surface fluxes and SST and found that such a negative feedback is scale dependent. On time scales of several days, high SST increases convective activities and enhances the surface evaporation (latent heat flux) to cool the sea surface, while in the climate scale the relationship between SST and latent heat flux becomes more complex due to the interaction with large-scale circulations causing the low-level convergence and decrease in the wind speeds.

The 5 day averaged adjustment of sensible heat flux as well as longwave and shortwave radiation fluxes is presented in Table 1. The increase of sensible heat is only 1.5 W/m^2 in response to the SST perturbation, being 1 order of magnitude smaller than the latent heat adjustment. Such a response is consistent with the low sensible heat flux and high latent heat flux in the tropics, as shown in the typical estimation of the Bowen ratio ~0.06–0.12 [*Jo et al*., 2004] in the Tropic Pacific.

3.1.2.2. Radiation Fluxes

Adjustments in shortwave and longwave radiation involve more complex feedback processes. When the perturbation-induced heat is released from the ocean primarily through the latent heat flux, it increases the heat and moisture input into the lower atmosphere. Figure 9 (top) presents the vertical structure of the zonally averaged (105E–110E) air temperature, which shows a general pattern of a southward increase and vertical decrease in temperature. The increase in temperature in the lower atmosphere due to the perturbation of sea surface temperature in case *I* is shown in the bottom plot, results from the heat release from the sea surface. When the heat was transferred from the ocean into the atmosphere, the temperature between the 8S and 8N and 16N and 20N has increased 0.1–0.4°C below the 850 hPa height over the shallow water regions in the Java Sea, Gulf of Thailand, and the shelf

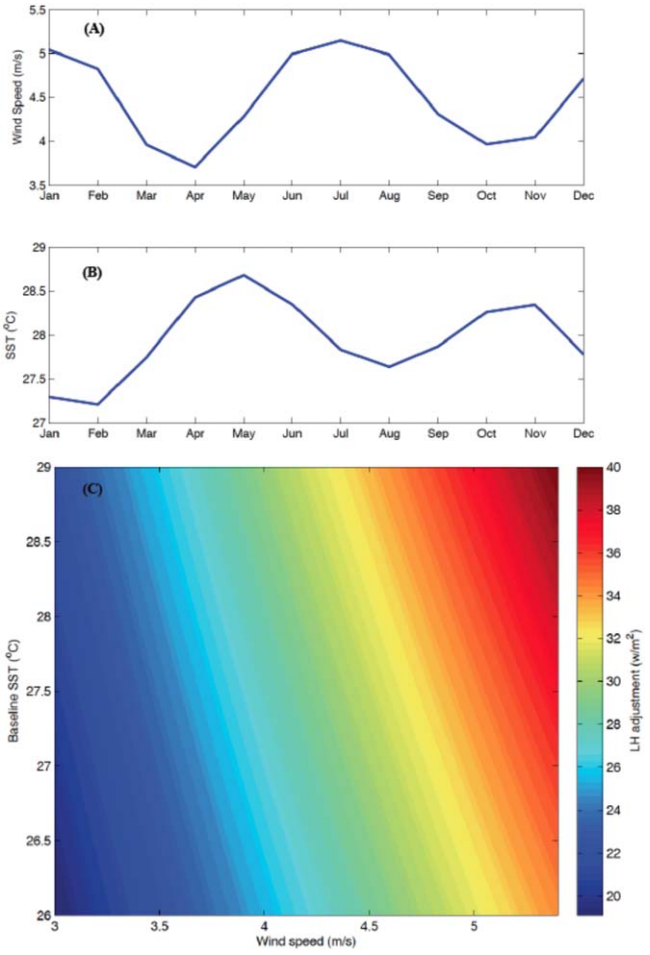

Figure 8. Climatological monthly mean (a) wind speed and (b) SST over the shallow water regions (water depth <200 m), derived from the NCEP long-term monthly mean wind speed (1981–2010) and OISST long-term monthly mean (1971–2000), respectively. (c) The magnitude of the latent heat adjustment with 1°C SST perturbation under different combinations of baseline of SST and wind speed.

of East China Sea, while the temperature over the unperturbed regions in the Indian Ocean (8S–20S) and land (8N–16N, 20N–30N) remains little changed.

More important, as the MC undergoes intensive atmospheric convective process, the increased latent flux (evaporation) enhances moisture input and the formation of convective clouds. Figure 10 shows the zonally averaged (105E–110E) cloud coverage with high-level clouds, low-level clouds, and clouds with vertical development. The low-level cloud coverage increased by 10–15% at the shallow water region due to enhanced moisture and thermal inputs, most of the which formed below 850 hPa. The low-level cloud is well known for its cooling effect due to a high albedo for reflection and warm temperature with strong infrared radiation to space. Consistent with an increase of low-level clouds over the shallow region when the positive SST perturbation strengthens the surface evaporation, an average decrease of 6.5 W/m^2 in shortwave radiation in 5 days occurs as low-level clouds act as a shield preventing incoming solar radiation to the sea surface, providing the second mechanism to restore the perturbed SST (Figure 11).

Unlike the latent heat adjustment, the magnitude of the adjustment of incoming solar radiation increases in the first 4 days, and then started to decrease afterward (Figure 11, bottom), as the formation of the convective clouds to the SST perturbation is not instantaneous. This suggests that although the latent heat adjustment and the solar radiation adjustment are inter-related as they are both linked to the surface evaporation process, the response time scale for each process is different.

It is worth noting that at the climate spatiotemporal scale, the sign of the low-level cloud feedback for climate change is still uncertain. While studies suggest that a climate warming can be associated with an increased low-level cloud cover and produce a negative cloud feedback [e.g., *Miller*, 1997; *Larson et al*., 1999; *Zhang and Bretherton*, 2008], other studies provide evidence for a positive low-level cloud feedback [*Clement et al*., 2009; *Brient and Bony*, 2013]. The uncertainty occurs as temperature changes that occur on seasonal to decadal time scales are often associated with both circulation changes and thermodynamics, which make it difficult to distinguish the part of cloud variations that results from a change in the dynamics or from the temperature change itself [*Bony et al*., 2004].

Table 1. The Adjustment of the Surface Heat Fluxes in Response to the SST Perturbation

Adjustment in Air-Sea Interactions	Latent Heat	Sensible Heat	Shortwave (Net)	Longwave (Net)	Longwave (Upward)	Longwave (Downward)
5 day average (W/m^2)	12.7	1.5	−6.3	−0.2	2.6	2.8
2 week average (W/m^2)	6.6	0.8	−4.4	−0.2	1.3	1.5

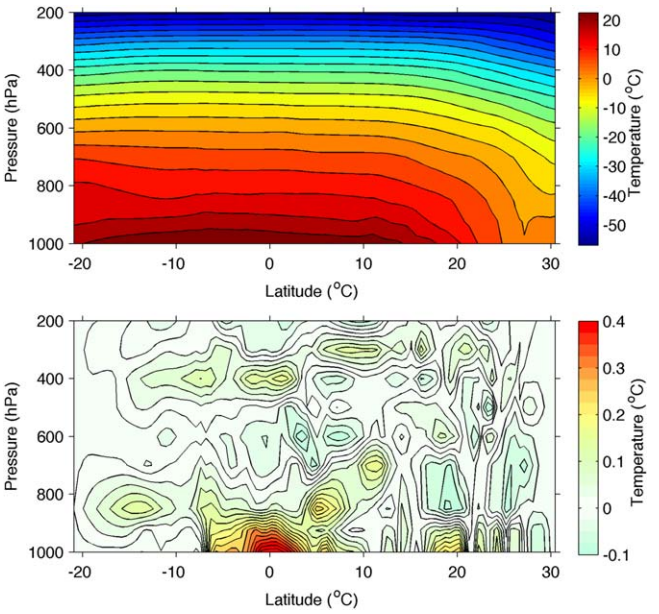

Figure 9. The zonally averaged (105E–110E) temperature structure in the (top) control run and (bottom) its change in case *I* shown as 5 day average after the water temperature perturbation.

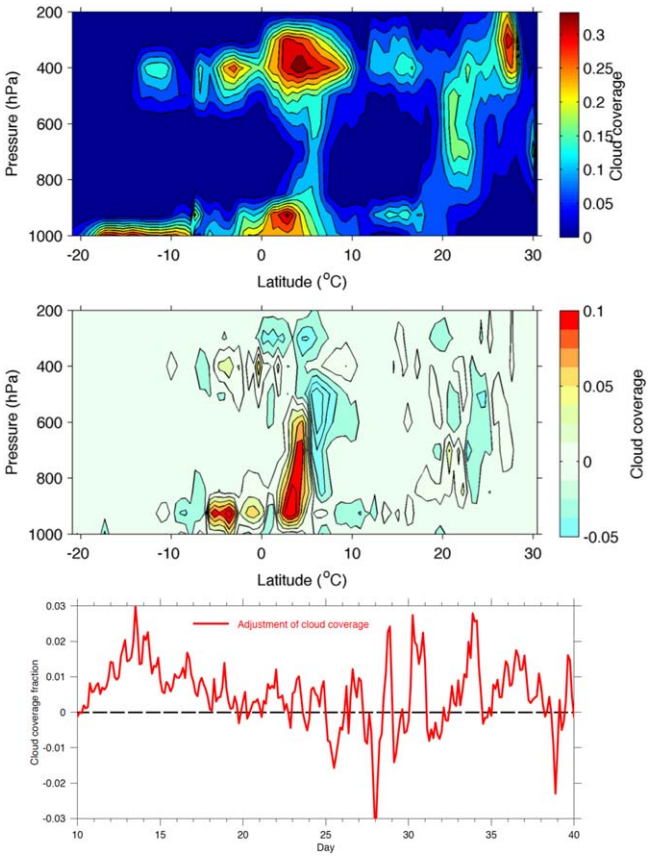

Figure 10. The zonally averaged (105E–110E) cloud coverage in the (top) control run and (middle) its change in case *I* shown as 5 day average after the water temperature perturbation and (bottom) the time series of the adjustment of lower-level cloud coverage below 850 hPa, averaged over the shallow water regions.

The longwave radiation plays a minor role in the adjustment of surface heat flux induced by SST perturbation. The net longwave radiation is -0.2 W/m^2, accounting for only 3% of total heat adjustment within 2 weeks (Table 1). Yet this is due to a counterbalance of the greenhouse gas effect, a positive feedback in the longwave radiation feedback. While the upward longwave radiation from sea surface increases by 2.6 W/m^2 following Stefan-*Boltzmann* Law; the increase in moisture input and cloud formation enhances the downward longwave radiation by 2.8 W/m^2, leaving a net effect of longwave radiation of -0.2 W/m^2.

The above analyses quantified the contribution of each component of surface fluxes in the negative feedback mechanisms. It is clear that the shallow water system can be dominated at short time scales by the local negative feedback process through "SST ↔ latent heat flux" adjustment and "SST ↔ low-level clouds reflecting incoming solar radiation" feedbacks. The coupled system restored SST significantly in the first 2 weeks after its initial perturbation, and both of these adjustments appear to be fluctuating afterward (Figures 7 and 11). The increased amount of the latent heat released from the ocean, as a response to the SST perturbation, is in total 4.3e^{19} J within 14 days, accounting for 58% of the total surface heat fluxes adjustment while the decreased amount of shortwave radiation absorbed by the ocean is -2.8e^{19} J, accounting for 38% of the total surface heat flux adjustment. This suggests that both of these processes are significant as mechanisms for the negative feedback over the shallow water regions of MC.

4. Sensitivity Analysis of Coupling Frequency

In the Ex#2, we altered the SST coupling frequency assuming time scales

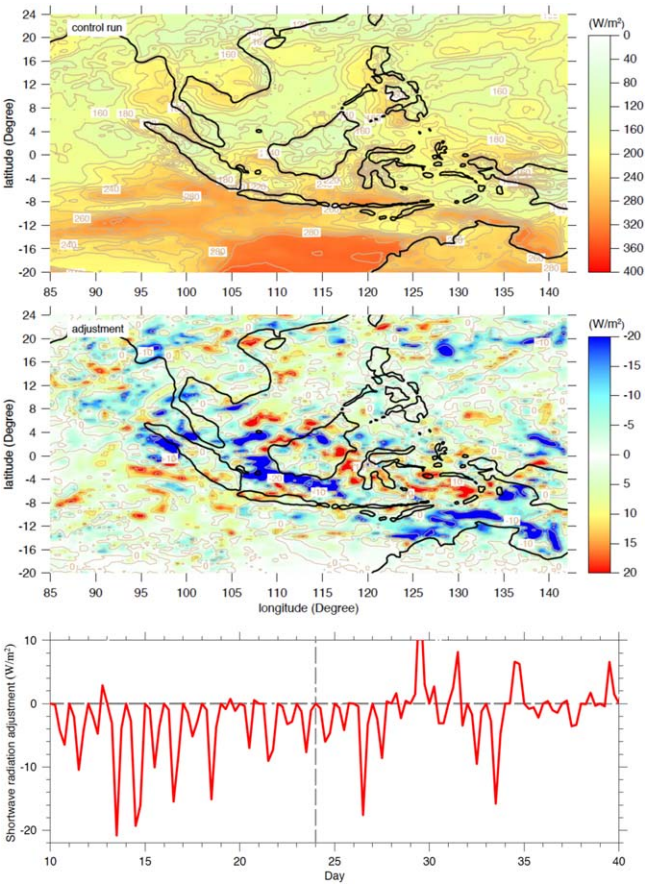

Figure 11. Distribution of the net shortwave radiation in (top) the control run, (middle) the increase in the latent heat flux 5 day average after initial water temperature perturbation in case *I*, and (bottom) the time series of the adjustment of the shortwave radiation averaged over the shallow water region.

for the coupling in the model that are higher or lower than the response time scale (3–5 day) of the identified air-sea feedback process with the aim of exploring the significance of resolving response time scale in a coupled model system (see experiment design in section 2). Results of Ex#2 show the differences of 10 year SST simulation results relative to the "control run" in case *a* and case *b*, averaged over the shallow water region (Figure 12). The results in case *a* (daily SST coupling) fluctuate around the "reference state" of the "control run" with errors $<\pm 0.07^{\circ}$C on average. In contrast to the fluctuation shown in case *a*, the model results in case *b* show a constant cold bias of $\sim -0.15^{\circ}$C with the maximum value reaching up to -0.3°C, indicating that the coupling error grows nonlinearly with the decrease of SST coupling frequency. In case *a*, the coupling error was negligible and randomly distributed with a noise level $<0.1^{\circ}$C. The error pattern in case *b*, however, is much more recognizable: the coupling error primarily arose from the shallow water regions, particularly during the boreal winter. The large errors were located in the Thailand and the adjacent shallow region of the South China Sea in the northern hemisphere, and the shallow water regions in the Java Sea, Timor Sea and Arafura Sea near Australia (Figure 13).

Ex#2 has shown that significant errors can develop under low SST coupling frequency at the shallow water regions. A spectral analysis (for node N_1 in Figure 1) shows that the SST at the shallow water regions oscillated at three dominant frequencies in the "reference state" (Figure 14a): a diurnal variation with a spectrum amplitude of $\sim 0.3^{\circ}$C, a semiannual variation with a spectrum amplitude of $\sim 0.8^{\circ}$C and an annual variation with a spectrum amplitude of $\sim 0.5^{\circ}$C. The strong semiannual variation and annual variation of SST have been long recognized by *Wyrtki* [1965] through harmonic analysis of SST of the tropical ocean and also identified through other approaches such as empirical orthogonal functions [*Clayson and Weitlich*, 2007]. The strong diurnal variation of SST in the tropical region resulting from solar radiation and the earth's rotation has been thoroughly reviewed by *Kawai and Wada* [2007].

In case *a*, the SST variation was also dominated by the same three oscillation frequencies, which explains why the simulation with a daily coupling of SST had a very similar result to that in the "control run." In case *b*, the weekly coupling of SST has induced an error that exhibited as an artificial oscillation with a period of $\sim$14 days (Figures 14b and 14c). This artificial oscillation with a spectrum amplitude of $\sim 0.2^{\circ}$C introduced the errors to the system, induced by the low frequency coupling.

The fact that low coupling frequencies induced artificial oscillations implies a dynamical connection between resolving air-sea feedback processes and the model coupling frequency. This confirmed our hypothesis on the significance of the negative feedback given the fact that these oscillations tend to

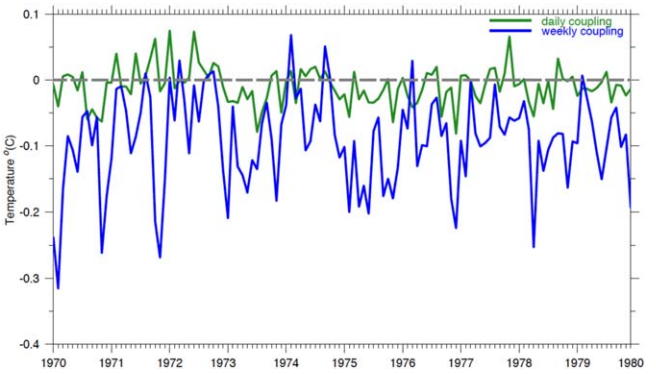

Figure 12. Time series of the error of monthly averaged SST for cases a and b in Ex#2 relative to the "control run," averaged over the shallow water regions.

develop only when coupling frequencies are lower than the inverse of the time scale of the feedback process. Considering a scenario that starts with an initial warm (cold) perturbation of SST: with the negative feedback mechanism, the coupled system adjusts surface heat fluxes to cool down (warm up) the ocean surface water from its perturbation and restore SST toward its equilibrium state. The magnitude of the adjustment of heat fluxes must be naturally attenuated during the progress of the SST restoration. When this process is simulated in a coupled model with low coupling frequency, which means that SST information in the atmospheric model is not updated for a period of time that is longer than the response time scale of the negative feedback process, this delay of the feedback would cause the surface water to be overcooled (overwarmed) from its warm (cold) perturbation and shoot to an opposite cold (warm) perturbation until the atmospheric model receives the updated SST information and starts to make another adjustment of the surface heat fluxes resulting again in overwarmed (overcooled) surface water. Such a process repeats itself every week in a weekly SST coupling experiment, resulting in a 14 day artificial oscillation (Figure 14c). The artificial oscillation can be negligible only if the coupling frequency is high enough so that the SST information is updated at a time interval shorter than the response time scale of the feedback process of ~3–5 days, as observed in the case *a*.

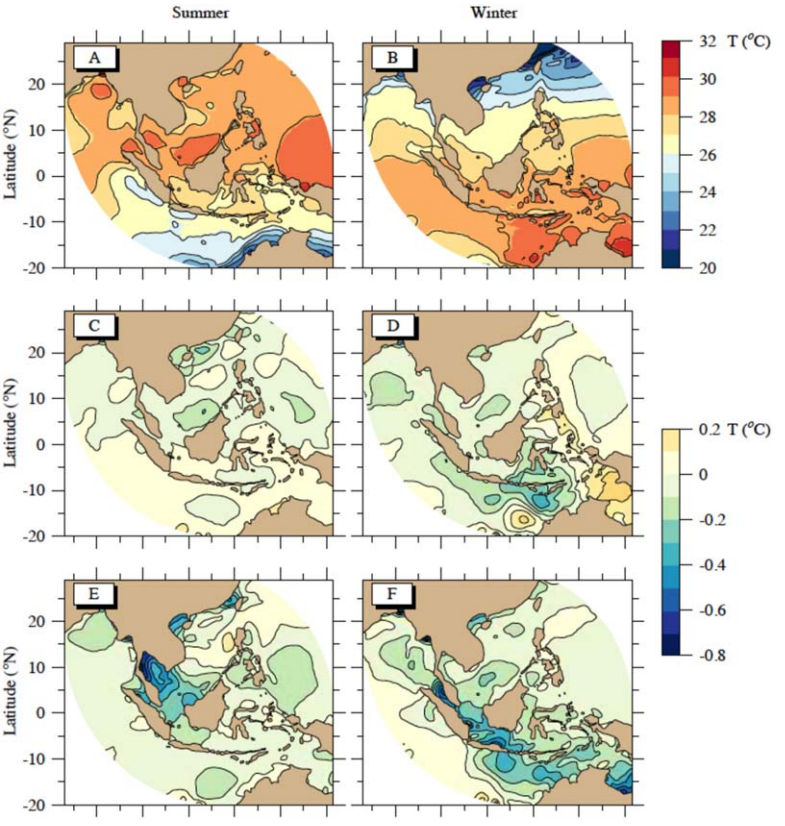

Figure 13. Distributions of the decadal-averaged boreal (a) summer and (b) winter SST from the "control run," and (c and e) the errors of the decadal-averaged summer SST for cases a and b in Ex#2 relative to the "control run"; and (d and f) the errors of the decadal-averaged winter SST for cases a and b relative to the "control run".

5. Discussions

5.1. Nature of Feedback Processes at Different Scales

From both oceanic and atmospheric point of view, the MC has a vitally important impact on global climate [*Neale and Slingo*, 2003] lying within the "Indo-Pacific warm pool" and as an "inter-ocean connection (mainly via Indonesia

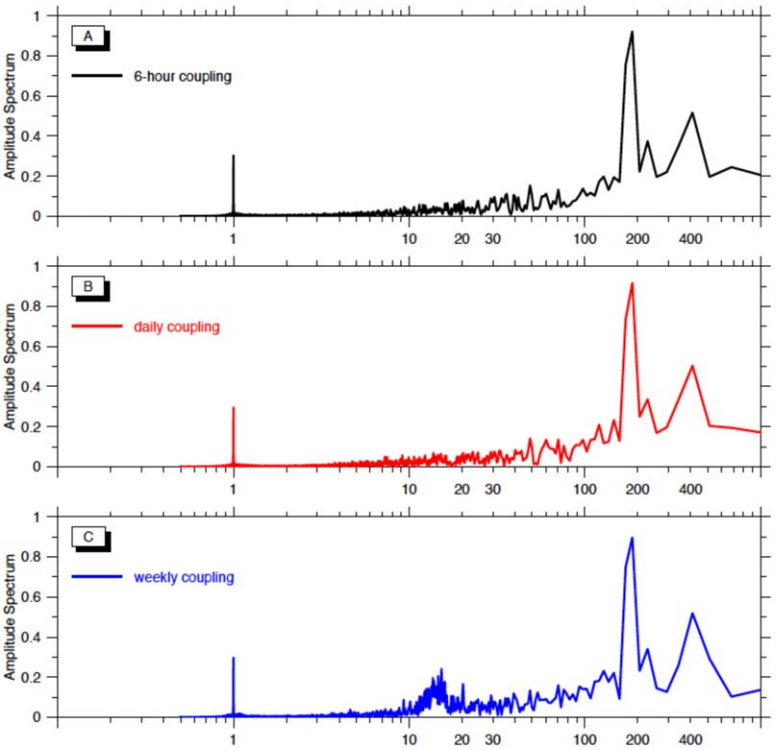

Figure 14. Amplitude spectrum for SST time series at node N_1, calculated from the 10 year SST times series with 6 h output interval. *X* axis is the distribution of oscillation period (unit: day) (i.e., 1/frequency).

Through Flow (ITF))." These previous studies clearly imply the connection of the MC to large-scale climate variability. *Wyrtki* [1987] proposed that the ITF across the MC is driven by the pressure gradient between the western Pacific and the eastern Indian Ocean and the transfer of tropical western Pacific waters and heat into the Indian Ocean is closely linked through air-sea interactions to coupled modes of ENSO, the Asian Monsoon, and the Indian Ocean Dipole (IOD) [*Gordon*, 2005; *Gordon et al*., 2012]. Other studies use GCM models and observations [*Yuan et al*., 2011, 2013; *Xu et al*., 2013] to demonstrate that the upwelling anomalies in the tropical eastern Indian Ocean during IOD events are able to penetrate into the equatorial Pacific Ocean through the Indonesian Seas around the MC and induce significant coupled evolution of the tropical Pacific oceanic and atmospheric circulations.

Not surprisingly, many studies have investigated the ocean-atmosphere processes relating the warm pool of the equatorial Indian and western Pacific (EIWP), within which the MC is located, to the other oceans with a focus on ENSO variability [*Alexander et al*., 2002; *Lau et al*., 2005; *Wang et al*., 2006; *Xie et al*., 2009; *Hong et al*., 2014]. As a trigger of local convection, the warm pool of the EIWP exhibits various positive feedback processes in the large regional and basin scales affecting ENSO variability. Using a hierarchy of reduced-physics models, *Wang and Xie* [1998] demonstrates the mean state of warm SST over the warm pool of EIWP favors unstable Kelvin and Rossby wave modes primarily through a coupled wind-entrainment-evaporation feedback and may sustain the Madden-Julian Oscillation. *Wang et al*. [2000] explains a teleconnection during ENSO between the Pacific and East Asia that is confined in the lower troposphere and demonstrates that the development and persistence of such teleconnection are primarily caused by a positive thermodynamic feedback between the large-scale western North Pacific anticyclone anomaly and the sea surface cooling in the presence of mean northeasterly trades. Similarly, a positive wind-evaporation-SST (WES) feedback in the central tropical Pacific that reinforces the initial meridional dipole of SST anomalies via surface evaporation and wind stirring that emphasizes the role of zonal easterly wind instead of meridional wind was proposed by [*Xie and Philander*, 1994; *Xie*, 2004]. Further, *Xie et al*. [2009] show that anticyclonic anomalies over the Northwest Pacific are forced not by local air-sea interaction [*Wang et al*., 2000; *Lau and Nath*, 2003], but remotely by Tropic Indian Ocean (TIO) SST, suggesting that the TIO warming serves as a capacitor

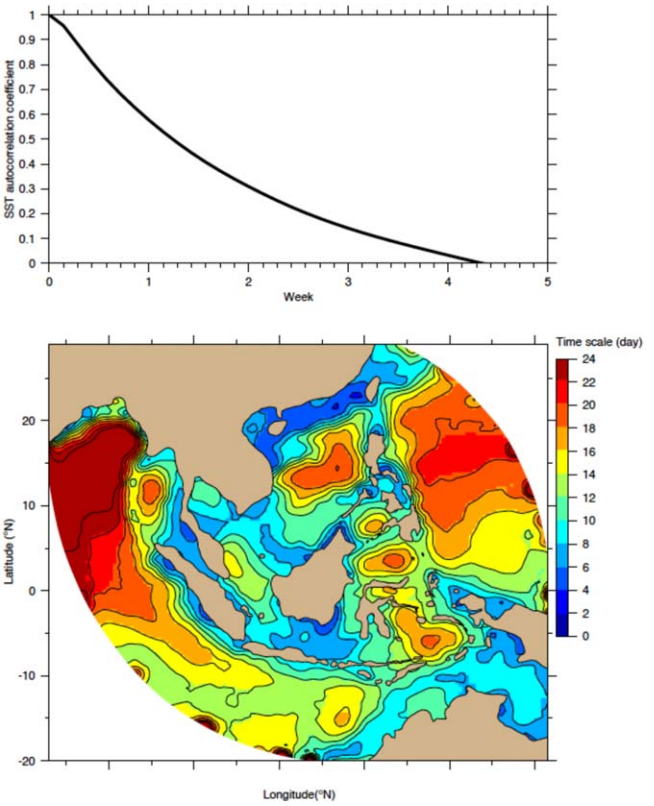

Figure 15. The decay of the autocorrelation over time for (top) the modeled domain-averaged SST and (bottom) the horizontal distribution of the decorrelation time scale of the modeled SST defined as the time scale for the autocorrelation coefficient reaches its e-folding value.

anchoring atmospheric anomalies over the Indo-western Pacific Oceans, emanating a warm Kelvin wave into the Pacific resembling the dynamics described by *Gill* [1980] model, which drives northeasterly winds onto the equatorial low pressure in the baroclinic Kelvin wave, inducing surface divergence and suppressing deep convection in the subtropical Northwest Pacific. Their results suggest that in the northwest Pacific, this equatorial Kelvin wave induces northeasterly surface wind anomalies, and the resultant divergence in the subtropics triggers suppression of Northwest Pacific convection and the anomalous anticyclone, explaining significant climate anomalies that persist through the summer (June-August) after El Nino dissipates in spring over the equatorial Pacific. Other studies [e.g., *Hong et al*., 2014, Figure 4] suggest that the teleconnection associated with a large-scale coherent pattern in sea level pressure, with high pressure over southern Australia and low pressure over the southern Pacific forming a large transverse cell through a positive feedback that adds on top of the Bjerknes instability to booster the growth of super El Niño.

In all large-scale ocean-atmosphere dynamics associated with ENSO and MJO, one can look for local sources of instability that support the growth and sustaining mechanism of atmospheric and oceanic patterns. It is natural to link convection to instability theories since convection is the major source of instability in the tropical region. One important requirement for resolving the above feedbacks is to allow for the generation and propagation of a planetary-scale Kelvin and Rossby wave structure and to build large regional scale or basin scale teleconnection through an "atmospheric bridge" or "ocean channel." Hence, GCMs or at least basin scale models are required. In addition, the investigated anomalies and perturbations are usually spatially sizeable (e.g., IOD, central pacific SST anomalies, NW pacific anticyclone anomaly) to identify their effects on climate variability with an intraseasonal and interannual time scale.

Here we emphasize that although the regional and global feedbacks between the MC and the rest of the world reviewed above are important, these feedbacks are not the focus of the present study. Instead, we focus on local-scale air-sea interactions over the shallow water region. Our regional model is set up to cover the MC and constrained by fixed atmospheric and oceanic lateral boundary conditions based on reanalysis data. One-time perturbations of SST are designed only for the shallow water region. In these experiments, we observe that the ocean and the atmosphere are tightly coupled over shallow water regions through a strong local negative feedback and primarily as a vertical process, within a short time scale of a few days. The present study also differs in its focus and scales of interest from other studies using regional models to examine the seasonal and intraseasonal variability (e.g., MJO) in the Pacific warm pools [e.g., *Waliser et al*., 1999; *Wang et al*., 2011; *Small et al*., 2011]. At the intraseasonal time scale, wind speed anomalies may give a much larger contribution to the evaporation signal than SST anomalies and both remote forcing and local circulation feedbacks [*Xie et al*., 2009] may amplify intraseasonal convection variability [*Small et al*., 2011].

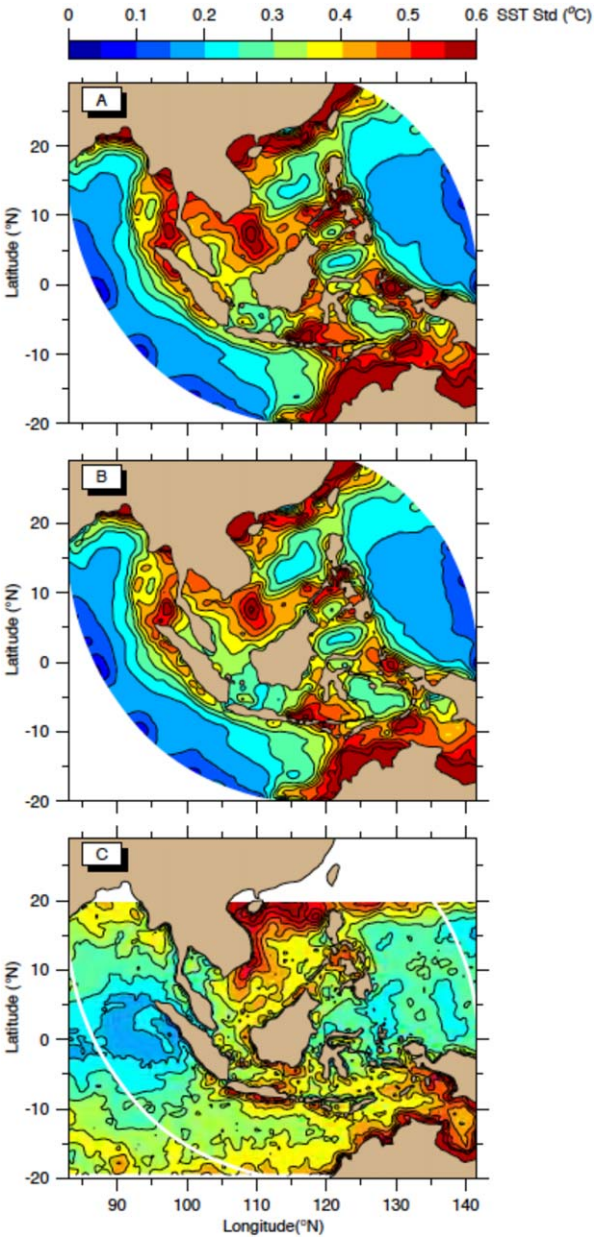

Figure 16. Distributions of the standard deviation of (a) model surface layer temperature, (b) model 6 m vertical averaged temperature, both are estimated from daily model results (1970–1979), and (c) the standard deviation of the daily SST data sets: RMASSA (only available for years 2008–2011, see section 2.2 for the description). A 60 day high-pass filter was applied to modeled/observed SST time series to remove seasonal signal prior to the calculation of standard deviation, so that the SST standard deviation here represents the short-term variability of SST.

5.2. Feedback Process and Model Coupling Frequency

Results have shown that the error primarily develops in the shallow water region when SST coupling frequency is low, while model performance in the open ocean, interestingly, appears to be less sensitive to the change in SST coupling frequency (Figure 13). Such distinct model responses in the shallow and deep water regions must be interpreted carefully. SST over the shallow water regions may have shorter a decorrelation time scale and therefore requires higher SST coupling frequency to resolve its temporal variability since they could be significantly influenced by local air-sea heat fluxes as well as submesoscale processes due to their smaller water volumes (Figure 15). In the open oceans, the ocean-basin scale circulations and other large-scale processes play important roles in regulating the variability of the water properties; hence, the SST variability could be characterized with a longer decorrelation time scale.

Due to the configuration of the vertical sigma coordinate, the thickness of the model surface layer varies according to local water depth with the thickest layer up to 6 m in the deepest region. In order to ensure that our analysis is physically meaningful, we examined water temperature profiles in the shallow water region where the water column at the upper 6 m is represented by multiple model layers. Results show that water at the upper 6 m is mostly well mixed. Accordingly, the short-term variability (i.e., standard deviation after removing its seasonal cycle) of the vertically averaged model temperature at the upper 6 m shows a very similar pattern to that of modeled SST (Figures 16a and 16b). This result provided us confidence that the SST patterns over shallow water regions reflect the physical phenomenon, rather than being an artifact caused by the varying thickness of model surface layer.

However, although the observed SST data set (Figure 16c, see section 2 for data description) agrees with model results to a certain extent showing a general pattern with larger SST short-term variation in the shallow water regions and smaller variation in the deep water regions, the SST short-term variability in deep water regions shown in the model simulation is significantly lower than that of the observed SST data set. This result led us to believe that the relatively coarse vertical resolution of the model surface layer at the deep water regions might have resulted in some underestimation of SST (intradaily) variability due to an

overestimation of the mixed layer depth, and consequently weakened the feedbacks in the deep waters, as implied by *Bernie et al*. [2008], *Ham et al*. [2010], and *Masson et al*. [2012]. Taking the results of these studies into account, we are confident in our results for the *targeted* shallow water regions, although the magnitude of SST variability in the open ocean may have been underestimated.

One question that has not been fully addressed is why the coupled model, when run at low coupling frequency, simulates an equilibrium temperature with a cold bias rather than a warm bias. We propose a hypothesis here that the fundamental mechanism behind this cold bias involves asymmetry in the negative feedback process, so that the restoring surface fluxes are more significant under relatively warm temperature perturbation than cold temperature perturbations. We speculate that the negative feedback operating during warm temperature departure from equilibrium accumulates more cooling fluxes, than the accumulated warming fluxes achieved by the same feedback process during the corresponding cold temperature departures, which would result in a cold temperature bias when running the coupled model at low coupling frequency over time. The reason we expect to see such an asymmetry in the negative feedback process stems from the nonlinearities evident in the physics of evaporation (Clausius-Clapeyron relationship), cloud formation (triggering of moist convection) and ocean convective mixing. Although it is beyond the research goal of this work, this hypothesis is worth a great deal of effort and should be tested in the future research.

6. Conclusions

Experiments were conducted to explore the local-scale air-sea feedback process and associated physical mechanisms over the shallow (shelf) water regions of the MC. Running the coupled/uncoupled models with perturbed SST fields, we identify that the targeted region could be dominated by a negative feedback process at a short time scale of several days through a local "SST $\leftrightarrow$ latent heat flux" adjustment and "SST $\leftrightarrow$ low-level clouds reflecting incoming solar radiation" adjustment. The energy budget shows that $\sim$38% of initial perturbation-induced heat was adjusted through the air-sea feedback mechanisms within 2 weeks, of which 58% is directly transferred into the atmosphere by the adjustment in latent heat flux due to the evaporative cooling mechanism. The increased inputs of heat and moisture into the lower atmosphere then modifies its thermal structure and increases the formation of low-level clouds, which act as a shield preventing incoming solar radiation from reaching the sea surface, accounts for 38% of the total adjustment of surface heat fluxes, serving as the second feedback mechanism to restore the perturbed SST. The adjustment of sensible heat flux (7%) and net longwave radiation ($-$3%) play a secondary role.

A set of experiments was carried out by alternating the coupling frequency of SST higher and lower than the response time scale of coupled feedback processes. Results of spectral analysis showed that modeling with daily or higher SST coupling frequency was able to resolve the SST temporal and spatial variabilities, while modeling with low coupling frequency of SST induced artificial oscillations as it failed to resolve the coupled ocean-atmosphere dynamics at the response time scale of the feedback process, resulting in cold bias in the SST simulation. The two-way air-sea feedback tightly links the surface heat fluxes, coulds, and SST, and can play an important role in regulating the short-term variability of the SST over the shallow shelf water regions, which are significantly influenced by local air-sea heat fluxes as well as submesoscale oceanic processes at shorter time scales. This work also shows the dynamical relations among the local air-sea feedback process, model coupling frequency, and the geometrical characteristics of the shallow water region of the MC. As the regional oceanic and atmospheric dynamics vary significantly in time and space, the approach used in this study can be valuable to understand the air-sea interactions in different shallow water systems.

Acknowledgments
This work was supported by the Singapore National Research Foundation (NRF) through the Center for Environmental Sensing and Monitoring (CENSAM) under the Singapore-MIT Alliance for Research and Technology (SMART) program. Wei's research was supported by National Natural Science Foundation of China (NSFC, 41106003). P.X.'s research was also supported by the Michigan Tech Research Excellence Fund-Research Seed Grant. We thank three anonymous reviewers' valuable comments, which have greatly helped us to improve this research. We also thank J.S. Pal and E.-S. Im for their valuable suggestions on this work.

References

Aldrian, E., D. V. Sein, D. Jacob, L. D. Gates, and R. Podzun (2005), Modeling Indonesian rainfall with a coupled regional model, *Clim. Dyn.*, *25*, 1–17.

Alexander, M. A., I. Blad, M. Newman, J. R. Lanzante, N. Lau, and J. D. Scott (2002), The atmospheric bridge: The influence of ENSO teleconnections on air-sea interaction over the global oceans, *J. Clim.*, *15*, 2205–2231.

Beggs, H., A. Zhong, G. Warren, O. Alves, G. Brassington, and T. Pugh (2011), RAMSSA—An operational, high-resolution, multi-sensor sea surface temperature analysis over the Australian region, *Aust. Meteorol. Oceanogr. J.*, *61*, 1–22.

Bernie, D. J., E. Guilyardi, G. Made, J. M. Slingo, and S. J. Woolnough (2007), Impact of resolving the diurnal cycle in an ocean-atmosphere GCM. Part 1: A diurnally forced OGCM, *Clim. Dyn.*, *29*, 575–590.

Bernie, D. J., E. Guilyardi, G. Madec, J. M. Slingo, S. J. Woolnough, and J. Cole (2008), Impact of resolving the diurnal cycle in an ocean-atmosphere GCM. Part 2: A diurnally coupled CGCM, *Clim. Dyn.*, *31*, 909–925.

Bjerknes, J. (1969), Atmospheric teleconnections from the equatorial Pacific, *Mon. Weather Rev.*, *97*, 163–172.
Bony, S., J.-L. Dufresne, H. Le Treut, J. Morcrette, and C. Senior (2004), On dynamic and thermodynamic components of cloud changes, *Clim. Dyn.*, *22*, 71–86.
Brient, F., and S. Bony (2013), Interpretation of the positive low-cloud feedback predicted by a climate model under global warming, *Clim. Dyn.*, *40*, 2415–2431.
Buck, A. L. (1981), New equations for computing vapor pressure and enhancement factor, *J. Appl. Meteorol.*, *20*, 1527–1532.
Chelton, D. B., and S.-P. Xie (2010), Coupled ocean-atmosphere interaction at oceanic mesoscales, *Oceanography*, *23*, 52–69.
Chen, C., H. Liu, and R. Beardsley (2003), An unstructured grid, finite-volume, three dimensional, primitive equations ocean model: Application to coastal ocean and estuaries, *J. Atmos. Oceanic Technol.*, *20*, 159–186.
Chen, C., R. C. Beardsley, and G. Cowles (2006), An unstructured grid, finite-volume coastal ocean model (FVCOM) system, special issue entitled "Advances in Computational Oceanography," *Oceanography*, *19*(1), 78–89.
Chen, C., et al. (2008), Physical mechanisms for the offshore detachment of the Changjiang Diluted Water in the East China Sea, *J. Geophys. Res.*, *113*, C02002, doi:10.1029/2006JC003994.
Chen, C., Z. Lai, R. C. Beardsley, Q. Xu, H. Lin, and N. T. Viet (2012), Current separation and upwelling over the southeast shelf of Vietnam in the South China Sea, *J. Geophys. Res.*, *117*, C03033, doi:10.1029/2011JC007150.
Clayson, C. A., and D. Weitlich (2007), Variability of tropical diurnal sea surface temperature, *J. Clim.*, *20*, 334–352.
Clement, A. C., R. Burgman, and J. R. Norris (2009), Observational and model evidence for positive low-level cloud feedback, *Science*, *325*, 460–464.
Christensen, J. H., et al. (2007), Regional climate projections, in *Climate Change, 2007: The Physical Science Basis. Contribution of Working Group I to the Fourth Assessment Report of the Intergovernmental Panel on Climate Change*, chap. 11, edited by S. Solomon et al., pp. 848–940, Cambridge Univ. Press, Cambridge, U. K.
Danabasoglu, G., W. G. Large, J. J. Tribbia, P. R. Gent, B. P. Briegleb, and J. C. McWilliams (2006), Diurnal coupling in the tropical oceans of CCSM3, *J. Clim.*, *19*, 2347–2365.
Fedorov, A. V. (2008), Ocean-atmosphere coupling, in *Oxford Companion to Global Change*, edited by A. Goudie and D. Cuff, pp. 369–374, Oxford Univ. Press.
Gianotti, R. L., and E. A. B. Eltahir (2013a), Regional climate modeling over the Maritime Continent. Part I: New parameterization for convective cloud fraction, *J. Clim.*, *27*, 1488–1503, doi:10.1175/JCLI-D-13-00127.1.
Gianotti, R. L., and E. A. B. Eltahir (2013b), Regional climate modeling over the Maritime Continent. Part II: New parameterization for autoconversion of convective rainfall, *J. Clim.*, *27*, 1504–1523, doi:10.1175/JCLI-D-13-00171.1.
Gianotti, R. L., D. Zhang, and E. Eltahir (2012), Assessment of the regional climate model version 3 over the maritime continent using different cumulus parameterization and land surface schemes, *J. Clim.*, *25*, 638–656.
Gill, A. E. (1980), Some simple solutions for heat-induced tropical circulation, *Q. J. R. Meteorol. Soc.*, *106*, 447–462.
Giorgi, F., and L. O. Mearns (1999), Introduction to special section: Regional climate modeling revisited, *J. Geophys. Res.*, *104*, 6335–6352.
Godfrey, J. S. (1996), The effect of the Indonesian throughflow on ocean circulation and heat exchange with the atmosphere: A review, *J. Geophys. Res.*, *101*, 12,217–12,237.
Gordon, A. L. (2005), Oceanography of the Indonesian seas and their through-flow, *Oceanography*, *18*(4), 14–27.
Gordon, A. L., B. A. Huber, E. J. Metzger, R. D. Susanto, H. E. Hurlburt, and T. R. Adi (2012), South China Sea throughflow impact on the Indonesian throughflow, *Geophys. Res. Lett.*, *39*, L11602, doi:10.1029/2012GL052021.
Ham, Y. G., J. S. Kug, I. S. Kang, F. F. Jin, and A. Timmermann (2010), Impact of diurnal atmosphere-ocean coupling on tropical climate simulations using a coupled GCM, *Clim. Dyn.*, *34*, 905–917.
Hartmann, D. L., and M. L. Michelsen (1993), Large-scale effects on the regulation of tropical sea surface temperature, *J. Clim.*, *6*, 2049–2062.
Hill, C., and J. Marshall (1995), Application of a parallel Navier-Stokes model to ocean circulation, in *Parallel Computational Fluid Dynamics: Implementations and Results Using Parallel Computers*, edited by A. Ecer et al., pp. 545–552, Elsevier Sci., N. Y.
Hong, L., L. Ho, and F. Jin (2014), A southern hemisphere booster of super El Niño, *Geophys. Res. Lett.*, *41*, 2142–2149, doi:10.1002/2014GL059370.
Isobe, A., and R. C. Beardsley (2006), An estimate of the cross-frontal transport at the shelf break of the East China Sea with the Finite Volume Coastal Ocean Model, *J. Geophys. Res.*, *111*, C03012, doi:10.1029/2005JC003290.
Jo, Y., X. Yan, J. Pan, W. T. Liu, and M. He (2004), Sensible and latent heat flux in the tropical Pacific from satellite multi-sensor data, *Remote Sens. Environ.*, *90*, 166–177.
Kalnay, E., et al. (1996), The NCEP/NCAR 40-year reanalysis project, *Bull. Am. Meteorol. Soc.*, *77*, 437–471.
Kawai, Y., and A. Wada (2007), Diurnal sea surface temperature variation and its impact on the atmosphere and ocean: A review, *J. Oceanogr.*, *63*, 721–744.
Koch-Larrouy, A., M. Lengaigne, P. Terray, G. Madec, and S. Masson (2010), Tidal mixing in the Indonesian Seas and its effect on the tropical climate system, *Clim. Dyn.*, *34*(6), 891–904, doi:10.1007/s00382-009-0642-4.
Kraus, E. B., and J. A. Businger (1994), *Atmosphere-Ocean Interaction*, 2nd Edition, 362 pp., Oxford University Press, N. Y.
Larson, K., D. L. Hartmann, and S. A. Klein (1999), The role of clouds, water vapor, circulation, and boundary layer structure in the sensitivity of the tropical climate, *J. Clim.*, *12*, 2359–2374.
Lau, N., and M. J. Nath (2003), Atmosphere-ocean variations in the Indo-Pacific sector during ENSO episodes, *J. Clim.*, *16*, 3–20.
Lau, N., A. Leetmaa, M. J. Nath, and H. Wang (2005), Influences of ENSO-induced Indo-Western Pacific SST anomalies on extratropical atmospheric variability during the boreal summer, *J. Clim.*, *18*, 2922–2942.
Lloyd, J., E. Guilyardi, and H. Weller (2011), The role of atmosphere feedbacks during ENSO in the CMIP3 models. Part II: Using AMIP runs to understand the heat flux feedback mechanisms, *Clim. Dyn.*, *37*(7–8), 1271–1292.
Marshall, J., C. Hill, L. Perelman, and A. Adcroft (1997), Hydrostatic, quasi-hydrostatic, and nonhydrostatic ocean modeling, *J. Geophys. Res.*, *102*, 5733–5752.
Masson, S., P. Terray, G. Madec, J. Luo, T. Yamagata, and K. Takahashi (2012), Impact of intra-daily SST variability on ENSO characteristics in a coupled model, *Clim. Dyn.*, *39*, 681–707, doi:10.1007/s00382-011-1247-2.
Meehl, G. A., R. Lukas, G. N. Kiladis, M. Wheeler, A. Matthews, and K. M. Weickmann (2001), A conceptual framework for time and space scale interactions in the climate system, *Clim. Dyn.*, *17*, 753–775.
Miller, R. L. (1997), Tropical thermostats and low cloud cover, *J. Clim.*, *10*, 409–440.
Neale, R., and J. Slingo (2003), The Maritime Continent and its role in the global climate: A GCM study, *J. Clim.*, *16*, 834–848.
Pal, J. S., et al. (2007), The ICTP RegCM3 and RegCNET: Regional climate modeling for the developing world, *Bull. Am. Meteorol. Soc.*, *88*, 1395–1409.

Qu, T., Y. T. Song, and T. Yamagata (2009), An introduction to the South China Sea throughflow: Its dynamics, variability, and application for climate, *Dyn. Atmos. Oceans*, *47*, 3–14.
Ramage, C. S. (1968), Role of a tropical "maritime continent" in the atmospheric circulation, *Mon. Weather Rev.*, *96*, 365–370.
Ramanathan, V., and W. Collins (1991), Thermodynamic regulation of ocean warming by cirrus clouds deduced from observations of the 1987 El Niño, *Nature*, *351*, 27–32.
Reynolds, R. W., N. A. Rayner, T. M. Smith, D. C. Stokes, and W. Wang (2002), An improved in situ and satellite SST analysis for climate, *J. Clim.*, *15*, 1609–1625.
Slingo, J. M., P. Inness, R. Neale, S. Woolnough, and G. Y. Yang (2003), Scale interactions on diurnal to seasonal time scales and their relevance to model systematic errors, *Ann. Geophys.*, *46*, 139–155.
Small, R. J., S. Xie, E. Maloney, S. de Szoeke, and T. Miyama (2011), Intraseasonal variability in the far-east pacific: Investigation of the role of air-sea coupling in a regional coupled model, *Clim. Dyn.*, *36*, 867–890.
Terray, P., K. Kamala, S. Masson, G. Madec, A. K. Sahai, and J. J. Luo (2011), The role of the intra-daily SST variability in the Indian monsoon variability and monsoon-ENSO-IOD relationships in a global coupled model, *Clim. Dyn.*, *39*(3–4), 729–754, doi:10.1007/s00382-011-1240-9.
Tillinger, D., and A. L. Gordon (2010), Transport weighted temperature and internal energy transport of the Indonesian throughflow, *Dyn. Atmos. Oceans*, *50*, 224–232.
Valcke, S., A. Caubel, R. Vogelsang, and D. Declat (2004), *OASIS3 User's Guide (oasis3_prism_2–4), PRISM Report 2*, 5th ed., Centre Européen de Recherche et de Formation Avancée en Calcul Scientifique (CERFACS), Toulouse, France.
Waliser, D. E., K. M. Lau, and J. Kim (1999), The influence of coupled sea surface temperatures on the Madden-Julian Oscillation: A model perturbation experiment, *J. Atmos. Sci.*, *56*, 333–358.
Wang, B., and X. Xie (1998), Coupled modes of the warm pool climate system. Part I: The role of air-sea interaction in maintaining Madden-Julian Oscillation, *J. Clim.*, *11*, 2116–2135.
Wang, B., R. Wu, and X. Fu (2000), Pacific-East Asian teleconnection: How does ENSO affect East Asian Climate?, *J. Clim.*, *13*, 1517–1536.
Wang, C., S.-P. Xie, and J. A. Carton (2004), A global survey of ocean-atmosphere and climate variability, in *Earth Climate: The Ocean-Atmosphere Interaction, Geophys. Monogr. Ser.*, vol. 147, edited by C. Wang, S.-P. Xie, and J. A. Carton, pp. 1–19, AGU, Washington, D. C.
Wang, C., W. Wang, D. Wang, and Q. Wang (2006), Interannual variability of the South China Sea associated with El Niño, *J. Geophys. Res.*, *111*, C03023, doi:10.1029/2005JC003333.
Wang, L., Y. Wang, A. Lauer, and S. Xie (2011), Simulation of seasonal variation of marine boundary layer clouds over the Eastern Pacific with a regional climate model, *J. Clim.*, *24*, 3190–3210.
Wang, W., and M. J. McPhaden (2001), Surface layer temperature balance in the equatorial Pacific during the 1997–98 El Niño and 1998–99 La Niña, *J. Clim.*, *14*, 3393–3407.
Wei, J., P. Malanotte-Rizzoli, E. Eltahir, P. Xue, D. Zhang, and D. Xu (2013), Coupling of a regional atmospheric model (RegCM3) and a regional oceanic model (FVCOM) over the Maritime Continent, *Clim. Dyn.*, *43*(5–6), 1575–1594, doi:10.1007/s00382-013-1986-3.
Weisberg, R. H., and L. Y. Zheng (2006), Circulation of Tampa Bay driven by buoyancy, tides, and winds, as simulated using a finite volume coastal ocean model, *J. Geophys. Res.*, *111*, C01005, doi:10.1029/2005JC003067.
Wyrtki, K. (1965), The annual and semiannual variation of sea surface temperature in the North Pacific Ocean, *Limnol. Oceanogr.*, *10*(3), 307–313.
Wyrtki, K. (1987), Indonesian through flow and the associated pressure gradient, *J. Geophys. Res.*, *92*, 12,941–12,946.
Xie, S. (2004), The shape of continents, air-sea interaction, and the rising branch of the Hadley circulation, in *The Hadley Circulation: Past, Present and Future*, vol. 21, edited by H. F. Diaz and R. S. Bradley, pp. 121–152, Springer, Netherlands.
Xie, S., K. Hu, J. Hafner, H. Tokinaga, Y. Du, G. Huang, and T. Sampe (2009), Indian Ocean capacitor effect on Indo-Western Pacific climate during the summer following El Niño, *J. Clim.*, *22*, 730–747.
Xie, S.-P., and S. G. H. Philander (1994), A coupled ocean-atmosphere model of relevance to the ITCZ in the eastern Pacific, *Tellus, Ser. A*, *46*, 340–350.
Xu, D., and P. Malanotte-Rizzoli (2013), Seasonal variation of the upper layer of the South China Sea and the Indonesian Seas: An ocean model study, *Dyn. Atmos. Oceans*, *63*, 103–130, doi:10.1016/j.dynatmoce.2013.05.002.
Xu, T., D. Yuan, Y. Yu, and X. Zhao (2013), An assessment of Indo-Pacific oceanic channel dynamics in the FGOALS-g2 coupled climate system model, *Adv. Atmos. Sci.*, *30*, 997–1016.
Xue, P., C. Chen, P. Ding, R. C. Beardsley, H. Lin, J. Ge, and Y. Kong (2009), Saltwater intrusion into the Changjiang River: A model-guided mechanism study, *J. Geophys. Res.*, *114*, C02006, doi:10.1029/2008JC004831.
Xue, P., C. Chen, R. C. Beardsley, and R. Limeburner (2011), Observing system simulation experiments with ensemble Kalman filters in Nantucket Sound, Massachusetts, *J. Geophys. Res.*, *116*, C01011, doi:10.1029/2010JC006428.
Xue, P., C. Chen, and R. C. Beardsley (2012), Observing system simulation experiments of dissolved oxygen monitoring in Massachusetts Bay, *J. Geophys. Res.*, *117*, C05014, doi:10.1029/2011JC007843.
Xue, P., C. Chen, J. Qi, R. C. Beardsley, R. Tian, L. Zhao, and H. Lin (2014), Mechanism studies of seasonal variability of dissolved oxygen in Mass Bay: A multi-scale FVCOM/UG-RCA application, *J. Mar. Syst.*, *131*, 102–119.
Yang, Z., and T. Khangaonkar (2009), Modeling tidal circulation and stratification in Skagit River estuary using an unstructured grid ocean model, *Ocean Modell.*, *28*, 34–49.
Yuan, D., J. Wang, T. Xu, P. Xu, Z. Hui, X. Zhao, Y. Luan, W. Zheng, and Y. Yu (2011), Forcing of the Indian Ocean dipole on the interannual variations of the Tropical Pacific Ocean: Roles of the Indonesian throughflow, *J. Clim.*, *24*, 3593–3608.
Yuan, D., H. Zhou, and X. Zhao (2013), Interannual climate variability over the Tropical Pacific Ocean induced by the Indian Ocean dipole through the Indonesian throughflow, *J. Clim.*, *26*, 2845–2861.
Zeng, X., M. Zhao, and R. E. Dickinson (1998), Intercomparison of bulk aerodynamic algorithms for the computation of sea surface fluxes using TOGA COARE and TAO data, *J. Clim.*, *11*, 2628–2644.
Zhang, G. J., V. Ramanathan, and M. J. McPhaden (1995), Convection-evaporation feedback in the equatorial Pacific, *J. Clim.*, *8*, 3040–3051.
Zhang, M., and C. Bretherton (2008), Mechanisms of low cloud-climate feedback in idealized single-column simulations with the community atmospheric model, version 3 (CAM3), *J. Clim.*, *21*, 4859–4878.
Zhao, L., C. Chen, J. Vallino, C. Hopkinson, R. C. Beardsley, H. Lin, and J. Lerczak (2010), Wetland-estuarine-shelf interactions in the Plum Island Sound and Merrimack River in the Massachusetts coast, *J. Geophys. Res.*, *115*, C10039, doi:10.1029/2009JC006085.
Zheng, L., C. Chen, and H. Liu (2003), A 3-D modeling study of the Satilla River estuarine system. Part I: Simulation of flooding/drying processes, *Estuaries*, *26*(3), 651–669.